ALCHEMY Jurnal Penelitian Kimia

Facile Synthesis of Composite Chitosan and *Durio zibethinus* Seed and Its Application as Adsorbent of Metal Ion Ni(II)

Silvia Devi Eka Putri, Sri Mulijani*, Komar Sutriah

Department of Chemistry, FMIPA, IPB University
Jalan Tanjung Kampus IPB, Dramaga, Babakan, Dramaga, Bogor, 16680, Indonesia

*Corresponding author: srimulijani@apps.ipb.ac.id

ABSTRACT. Nickel is the one of the most dangerous heavy metals that impact water ecosystems and human health. In this study, natural and harmless composite materials such as biochar and chitosan were modified to build adsorbent composites and form optimal conditions for the adsorption of nickel heavy metal ions from contaminated wastewater. Biochar was prepared from *Durio zibethinus* seeds by hydrothermal method to form nanopowder. It was treated with acid, while chitosan was designed as nanopowder by hydrothermal method, also without acid treatment. Composite adsorbents were prepared by mixing biochar and chitosan with a ratio of 4:3 (w/w). Fourier Transform Infrared characterizes composite materials as adsorbents, biochar, and chitosan. The surface morphology of the adsorbent was evaluated by scanning electron microscopy. Furthermore, Langmuir, Freundlich, and Temkin isotherms determine the adsorbent's performance. In addition, batch adsorption experiments were carried out to measure the effect of solution pH, adsorbent dosage, and initial concentration of metal ions. Nickel ion adsorption by the composite adsorbent showed an adsorption capacity of 26.69 mg/g, a maximum removal efficiency of 89.39% at optimum conditions of pH 6, an adsorbent dose of 0.5 g, and a contact time of 200 minutes. This adsorption capacity was better than chitosan and durian seed adsorbents. The nickel ion adsorption process by composite adsorbent shows a pattern in the Temkin isotherm model. In contrast, the chitosan and *Durio zibethinus* seed adsorbents tended to follow the Langmuir and Freundlich isotherm models. In addition, the adsorption kinetics of the composite material showed pseudo-second-order kinetics, and the reaction was exothermic.

INTRODUCTION

The release of heavy metals from industry into the environment has resulted in many problems for both human health and aquatic ecosystems (Alkherraz *et al.*, 2020). Nickel metal is one of the most toxic heavy metals due to its bioaccumulation in the food chain (Sinyeue *et al.*, 2022). This matter can be harmful to body cells, damaging the lungs, liver, and kidneys and causing skin dermatitis (Gillmore *et al.*, 2020). Therefore, the regulation of the Minister of Environment and Forestry Number 5 of 2022 stipulates that the maximum permissible concentration of Nickel ions in industrial wastewater is 0.5 mg/L. Many methods have been investigated to address the increasingly severe nickel pollution, including chemical deposition, ion exchange, and reverse osmosis (Wu *et al.*, 2019; El Mouhri *et al.*, 2020; Pohl, 2020). However, these methods have disadvantages, such as being relatively expensive, using too extensive chemicals, and being less efficient and effective at low concentration levels (Liao and Huang, 2019; Pavithra *et al.*, 2021). Therefore, new investigation methods for metal processing are still complicated and essential.

One of them is using an adsorbent in the adsorption method, which is widely recognized as the most effective and profitable way to reduce the amount of metal ions in water since this method stands out by its high capacity and effectiveness, low cost, environmental compatibility, and potential for regeneration (Al-Ghouti *et al.*, 2019; Boeykens *et al.*, 2019). Several adsorbent materials, especially organic wastes, have been studied to remove heavy metal ions, one of which is chitosan. Chitosan is a polysaccharide biopolymer with many amino and hydroxyl groups, making chitosan a potential material for heavy metal adsorption (Pam *et al.*, 2023).

Several researchers revealed promising results using chitosan in heavy metal remediation. Due to its chemical structure, chitosan has been used in removing pollutants such as heavy metal ions Cu(II), Cr(VI) (Anush *et al.*, 2020; Reis *et al.*, 2021), and Co(III) (Shahnaz *et al.*, 2020). Chitosan is also an efficient and sustainable dye remover (Abdelbasir *et al.*, 2021). However, Zhu *et al.* (2021) argue that when chitosan is applied as an adsorbent directly, it has a small surface area, so the adsorption capacity is low. The effectiveness of this single chitosan can be effectively increased by forming it into a composite. Agricultural waste such as durian seeds is a well-known fruit grown and consumed locally and for export, especially in Southeast Asian countries (Muaz *et al.*, 2014). Approximately 70% – 85% of the fruit is disposed of as waste and will become an environmental problem if not disposed of properly (Chua *et al.*, 2023). Therefore, reducing this agricultural waste by reusing it and using it as a pollutant remover is important.

Durian seeds contain cellulose, hemicellulose, and lignin fibers, which are held together by β 1-4 glycosidic bonds (Lestari *et al.*, 2022), making them able to trap water pollutants and also because of their macro-porous properties and resistance to temperature, pH, mechanical stress, and prolonged water immersion (Payus *et al.*, 2019). So that it can improve the physicochemical properties of chitosan, making it an efficient composite in removing the heavy metal Ni(II). The development of chitosan composites has been reported in several studies. Adding biopolymer to biochar is an efficient way to combine and improve the characteristics of the two solids. Biochar is the perfect support in configuration due to its structural advantage and high surface area. In contrast, chitosan is a source of chelating sites for pollutant molecules because of the NH_2 and O–H groups (Zhang *et al.*, 2018).

Hydrothermal modification is the process used. The hydrothermal carbonization process is one of many methods used to process composites and turn them into solid carbonized materials. It is a sustainable and alluring method because it is affordable, energy efficient, and uses air as a solvent as the reaction medium (Hammi *et al.*, 2020). Temperatures between 180 – 250 °C are used for hydrothermal processes under autogenous pressure. Additionally, it heats up at a pace of 5 – 10 °C/min and takes between 5 – 12 hours (Adolfsson *et al.*, 2020). According to (Heidari *et al.*, 2019), this process entails many intricate processes, including dehydration, decarboxylation, decarbonization, deamination, polymerization, condensation, and depolymerization. This reaction results in a porous structure and surface functionality that can provide an efficient adsorption capacity (Nunes *et al.*, 2019; Kafle, 2020)

MATERIALS AND METHODS

Chitosan (DD 70%) was procured from commercial; durian seeds were collected from the local market in Jambi. All materials related to chemical substances were procured from Merck, such as CH_3COOH (100% glacial Merck), NaOH (Merck), HCL (37%, Merck), $NiSO_4.6H_2O$, H_2SO_4 95–97% (Merck), $K_2S_2O_8$ (Merck), $Na_2C_4H_4O_6$, alkaline dimethylglyoxime (DMG). All of the reagents and chemicals purchased were of pro-analytical grade.

Synthesis of Hydrothermal Chitosan/Durian Seeds Composite Beads

A total of 4 g of chitosan powder with a DD of 70% was dissolved in 100 mL CH_3COOH 2% (v/v), and the solution was stirred for 2 hours at 60 °C. Furthermore, 3 g of durian seed powder was added and stirred up to homogeneous. After that, the solution was dropped into 200 mL NaOH 0.5 M to get the composite beads chitosan/durian seeds. Finally, the filtrate was treated in deionized water until it was neutral. Then, the mixed beads shifted to a 100 mL Teflon-lined stainless-steel autoclave, which was heated to 180 °C for 8 hours. The autoclave was promptly cooled after the procedure, and the solid product was collected and washed several times with distilled water until pH 7. The resulting solid materials were dried at 60 °C for 24 hours and named composite beads.

Optimization of Parameters

Ni(II) solution containing 50 mL with a concentration of 25 mgL^{-1}, the pH was adjusted with 2, 4, 6, and 8 variations using 0.1 M NaOH and 0.1 HCL solution. Then 0.1 g of chitosan powder, durian seeds, and composites, and adsorption was carried out at 250 rpm for 15 minutes. After that, the solid was separated, and the filtration was analyzed by UV-Vis spectrophotometry.

Determination of Performance of Adsorbent

The performance of the adsorbent was evaluated by the effect of adsorbent dosage, contact time, and initial concentration. The effect of chitosan, durian seed, and composites adsorbent doses was studied with variations of 0.1, 0.2, 0.3, 0.4, and 0.5 g. Various amounts of adsorbent were mixed into 50 mL of Ni(II) with a concentration of 25 mg L^{-1}. The solution is adjusted to the optimum pH determined by previous experiments. Then, the adsorption was performed at 250 rpm for 15 minutes. The solids were then separated, and the filtration was analyzed by UV-Vis spectrophotometry.

The effect of contact time was determined within the time range of 30 – 600 min. The optimum adsorbent dose of the chitosan, durian seed, and biochar powder obtained from the previous experiment was added into 50 mL of 25 mg L^{-1} Ni(II) solution at the optimum pH. The adsorption was conducted for 30, 45, 60, 75, 150, 225, 300, 375, 450, and 600 min. The solid material was then separated, and spectrophotometry UV-Vis analyzed the filtration.

To evaluate the effect of initial concentration was conducted by adding ion Ni(II) solution with concentrations of 60, 120, 180, 240, and 300 mg L^{-1} into adsorbent. The adsorption took place during the duration of the optimum time, which was determined in the prior experiment. Next, the solid material was separated, and the filtration was analyzed by UV-Vis spectrophotometry.

The adsorption efficiency and capacity at various times (qt) and equilibrium (qe) were calculated using Equation (1 and 2).

$$\text{Adsorption efficiency (\%)} = \frac{Co - Ce}{Co} 100\% \tag{1}$$

The final and initial Ni(II) concentrations in mgL^{-1} are denoted by Ce and Co, respectively.

$$\text{Adsorption capacity (Qe)} = \frac{(Co - Ce)}{m} V \tag{2}$$

The weight of the adsorbent in mg and the volume of the solution in mL are indicated by the letters M and V, respectively. Ce stands for the equilibrium Ni(II) concentration.

Determination of Ni(II) Contaminant

Ni(II) concentration was determined using the color-developing method with spectrophotometer UV-Vis measurement at a maximum wavelength of 470 nm, as reported by (Kristianto *et al.*, 2019). In brief, a 2 mL aliquot of the sample was transferred into a 50 mL measuring flask. Subsequently, 1 mL of 1 M H_2SO_4, 2 mL of 20% $Na_2C_4H_4O_6$, 8 mL of 5% $K_2S_2O_8$, 0.5 mL of 1% alkaline dimethylglyoxime (DMG), and 2.5 mL of 5 N NaOH were added, and distilled water was sequentially added to bring the total volume up to 50 mL. Before spectrophotometer testing, these mixes were allowed to sit for 30 min for color development. A calibration curve with standard solutions determined the Ni(II) concentration in the sample.

Evaluation of Kinetic Adsorption of Ni(II)

The kinetics of Ni(II) adsorption were calculated using pseudo-first-order Equation (3) and pseudo-second-order Equation (4).

$$\ln(q_e - q_t) = \ln q_e - K_1 t \tag{3}$$

$$\frac{t}{q_t} = \frac{1}{K_2\, qe^2} + \frac{1}{q_e} t \tag{4}$$

The rate constants for the pseudo-first and pseudo-second-order equations are k$_1$ (min^{-1}) and k$_2$ (mg.g^{-1} min^{-1}).

Determination of Isotherm of Adsorption

The Langmuir, Freundlich, and Temkin models Equations (5, 6, and 7), respectively) were used to model the Ni(II) adsorption isotherm.

$$\frac{C}{qt} = \frac{1}{q_{max}} C + \frac{1}{q_{max} K_L} \tag{5}$$

$$\ln q_t = \frac{1}{n} lC + \ln K_F \tag{6}$$

$$q_t = B \ln C + B \ln A \tag{7}$$

Ce (mg/g) is the equilibrium Ni(II) concentration, q$_e$ (mg/g) is the adsorbed Ni(II) per unit adsorbent weight, and K$_L$ is the Langmuir constant, which measures the adsorption energy and is related to the contact sites. The

Langmuir constant is K_L, and q_m is the monolayer adsorption capacity, shows the isotherm type so that $R_L = 0$, $0 < R_L < 1$, and $R_L > 1$, respectively, represent an irreversible, desirable, and undesirable isotherm. K_f shows the adsorption capacity ($mg^{1-1/n}/L^{1/n}/g$), and $1/n$ is the Freundlich constant, dependent on the adsorption capacity and surface adsorption intensity. A represents the equilibrium binding constant of the Temkin isotherm, and B is the Temkin constant related to heat adsorption (J/mol^{-1}).

Adsorption of Ni(II) Thermodynamics

A total of 0.5 g of each adsorbent was added to a 50 mL Ni(II) solution with starting concentrations of 25, 50, 75, and 100 mL (optimum pH) for 60 minutes at temperatures of 30, 40, and 50 °C. The adsorbent was filtered and examined using a UV-Vis Spectrophotometer with a wavelength of 470 nm after the experiment was completed. The Gibb's free energy ($\Delta G°$), enthalpy change ($\Delta H°$), and entropy change ($\Delta S°$) are calculated using the Equation (8 and 9) (Wang *et al.*, 2020).

$$\Delta G° = -RT \ln K_{MLF} \tag{8}$$

$$\ln K_{MLF} = \frac{\Delta S°}{R} - \frac{\Delta H°}{RT} \tag{9}$$

K_{MLF} stands for the ML^{-F} constant (which is a dimensionless parameter). The van't Hoff equation was used to calculate the standard enthalpy change ($\Delta H°$) and the standard entropy change ($\Delta S°$).

RESULTS AND DISCUSSION

Morphology of Adsorbent

The surface morphological structure of the chitosan/durian seed composite adsorbent was analyzed using SEM both before and after Ni(II) metal ions adsorption. Figures (1a and 1b) depict the surface morphology of the chitosan/durian seed composite adsorbent. The surface has a smooth and slightly rough texture, with particles that tend to be granular and somewhat porous, according to the results of the SEM study. The chitosan/durian seed composite has an average diameter of 96.86 µm, according to the examination of the size distribution of the pores performed using image program J, which shows that the composite is macroporous. The percentage study of porosity was analyzed using Origin software before Ni(II) metal absorption was 72.43% and dropped to 67.84% after absorption, demonstrating that Ni(II) ions had covered part of the surface.
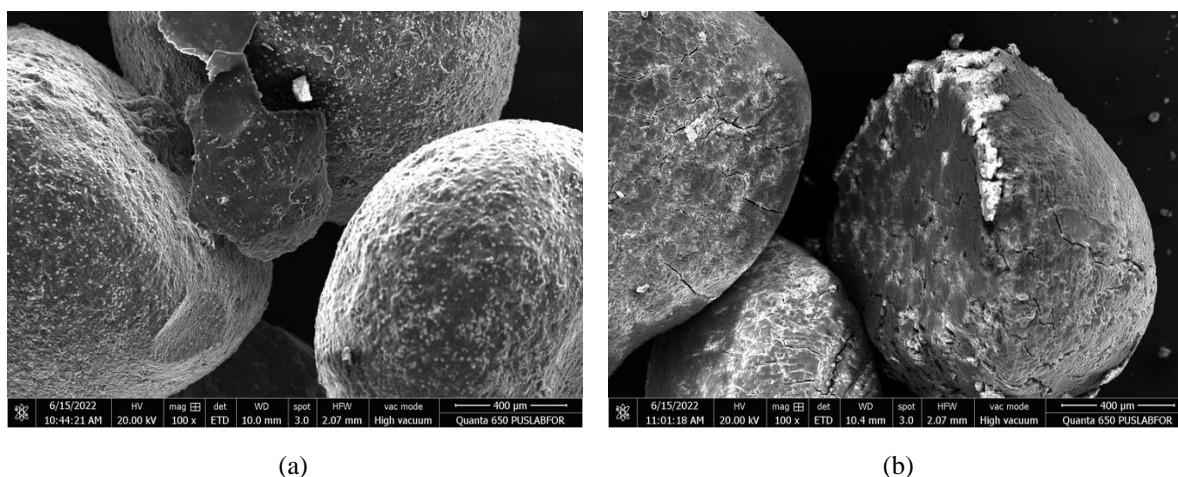

| (a) | (b) |

Figure 1. Morphology image of (a) composite before adsorption of Ni(II) ions, (b) composite after adsorption of Ni(II) ions.

Composite Beads

The solubility process of chitosan takes place through a protonation reaction (Abouhussein *et al.*, 2016). as shown in Figure 2. The amine group in chitosan will accept H^+ released by acetic acid to become positively charged ($-NH_3^+$). The formation of these ions causes chitosan to become dissolved. This process aims to enlarge the pore size of chitosan. Enlarged pores on chitosan will cause the $-NH_2$ group to have a higher affinity, thus increasing the ability to adsorb heavy metals (Rahayu, 2016).
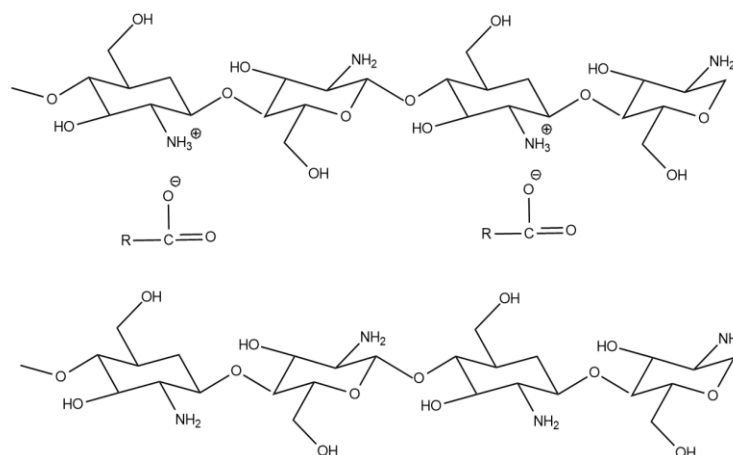
Figure 2. Chitosan protonation reaction.

Chitosan, dissolved in acetic acid, then added with durian seeds. The addition of durian seeds will make chitosan more stable against acid. Chitosan/durian seeds that have been homogenized then dripped into NaOH solution to form granules. When the chitosan solution drips into NaOH, chitosan re-polymerization occurs, expecting the chitosan polymer to be more organized so that the structure is more regular (Basir *et al.*, 2017). In the next stage, the adsorbent in the granules form rinsed with distilled water until it reaches neutral pH to remove NaOH.

Furthermore, Chitosan granules/durian seeds were put into the autoclave at 180 °C below autogenous pressure for 8 hours. This process aims to produce a structure of porous adsorbents, enhancing the adsorbable surfaces functionality. It provides efficient absorption capacity, increasing the ability to adsorb various contaminants, especially Ni(II) metal.

Phenomenon Adsorption
Impact of pH

The adsorption pH determines the adsorbents surface properties in terms of charge surface, ionization of functional groups, and the degree of dissociation of functional groups present on the adsorbent active site (Poonam *et al.*, 2018). Figure 3 shows that the adsorption capacity of Ni(II) metal ions increases with increasing pH. At pH 2 to 4, many hydrogen ions can bind to the active amine group (–NH₂) of chitosan and the active hydroxyl group (–OH) from durian seeds, resulting in competition between Ni(II) metal ions and ions hydrogen to occupy the active site (–NH₂) and (–OH), resulting in opportunities for the adsorption capacity of Ni(II) metal ions is decreasing (Liakos *et al.*, 2021). On the other hand, with increasing pH, the number of OH⁻ ions will increase; thus, the interaction of Ni(II) metal ions gets stronger (Kulkarni *et al.*, 2022).
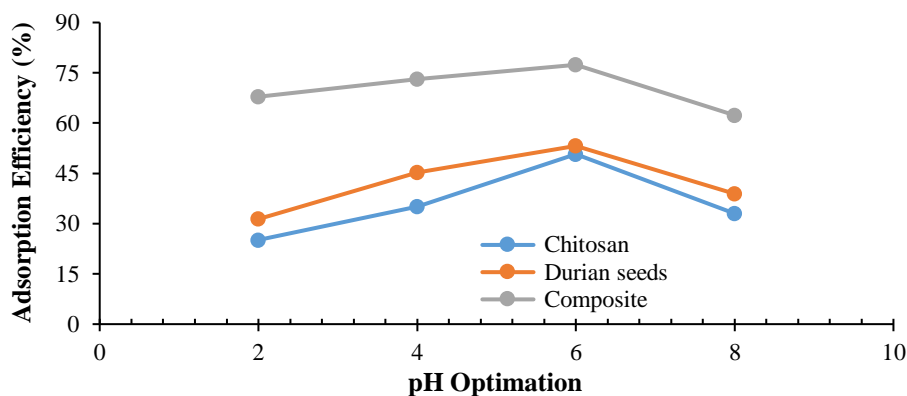

Figure 3. Adsorption efficiency of Ni(II) using chitosan adsorbent, durian seed adsorbent, and chitosan/durian seed composite on various pH variations.

Adsorption capacity is reduced when a pH is more than 6, due to the formation of hydroxide precipitates from Ni to Ni(OH)₂. Therefore, the pH of 6 was chosen as the optimal pH for the adsorption of Ni(II) metal ions

from aqueous solutions using chitosan adsorbent, durian seed, and chitosan/durian seed composite hydrothermal because the number of H^+ protons and OH^- ions may be relatively balanced so that it will bind more optimally with Ni(II) metal ions.

The adsorption efficiencies of Ni((II) on chitosan, durian seed, and the chitosan/seed composite are 50.70%, 53.18%, and 77.37%, respectively. Similar results were reported by (Kayalvizhi *et al.*, 2022), who studied the adsorption of Ni^{2+} from aqueous solutions by sawdust/chitosan nanocomposite; the optimal pH was found at pH 6. At pH value <6, a high concentration of H^+ ions competes with Ni^{2+} ions for sites active on the positively charged surface of the adsorbent. When the pH increases, the effect competition for H^+ ions decreases, and Ni^{2+} ions have an electrostatic attraction with the surface of the adsorbent negatively charged; this allows the process favorable for the adsorption of metal ions.

Performance of Adsorption Capacity

Ni(II) adsorption was studied by varying the adsorbent dose from 0.2 g to 0.6 g, keeping other parameters constant. Figure 4 shows that the percentage of Ni(II) ion removal increased with the amount of adsorbent. The increasing dose of chitosan/durian seed composite adsorbent is proportional to the increase in particles and surface area adsorbent, increasing the binding site number for metal ions and, therefore, the absorption efficiency also increases (Ifijen *et al.*, 2020). However, each adsorption capacity of chitosan and durian seed adsorbent decreased with increasing the amount of adsorbent due to the adsorbent agglomeration, resulting in covering the adsorbent pores, and therefore, their adsorption capacities can not perform at optimum.
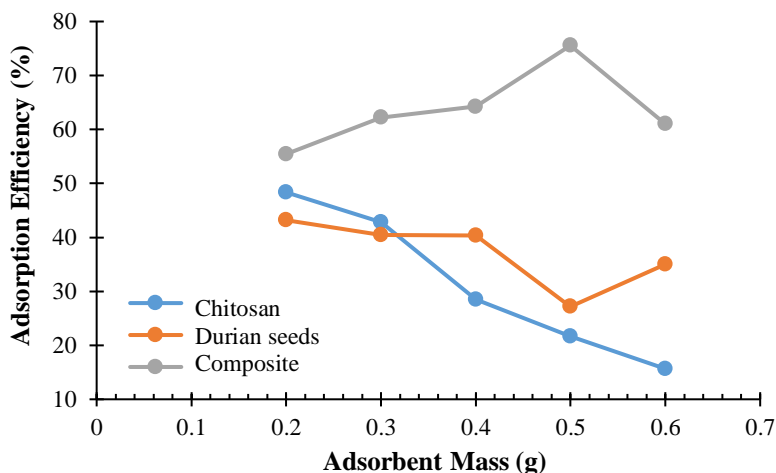

Figure 4. Adsorption efficiency of Ni(II) using chitosan, adsorbent durian seeds, and composite on various adsorbent dosage variations.

Figure 5 shows that the optimum mass of each adsorbent is 0.2 g for chitosan adsorbent and durian seed adsorbent and 0.5 g for chitosan/durian seed composite adsorbent. The maximum absorption efficiency of the chitosan/durian seed composite adsorbent is 75.54%, compared to chitosan and durian seed adsorbents were obtained at 48.34% and 43.18%.

Impact of Contact Time and Adsorption Kinetics

Contact time is the time required by the adsorbent to adsorption or bind to Ni(II) metal ions in the adsorption process, and this aims to determine the optimum time conditions of the adsorbent in adsorption Ni(II) metal ions until it reaches a balance point. Figure 5 shows the effect of contact time on the adsorption capacity of chitosan, durian seeds, and chitosan/durian seed composite to Ni(II) ions. As shown in Figure 5, it is observable that high adsorption capacity occurs early because the active site on the adsorbent is still available; therefore, Ni(II) ions easily attach to its adsorbent surface and let the adsorption capacity increase gradually with increasing time contact. After reaching equilibrium, a saturation process occurs, in which the adsorbent can no longer adsorb metal ions. According to the previous study (Al-Ghamdi, 2022), the adsorption process occurs in two stages. In the first stage of the mechanism, many adsorption sites are available on the surface adsorbent. However, the areas become

202

saturated at the end of adsorption, thereby limiting adsorption. The adsorption equilibrium occurs for the chitosan adsorbent from 75 min and decreases at 375 min; meanwhile, the equilibrium for durian seed adsorbent occurs from 225 min and drops at 300 minutes. In contrast, the adsorption efficiency gradually increases to equilibrium from 60 min to 300 min for the composite adsorbent.
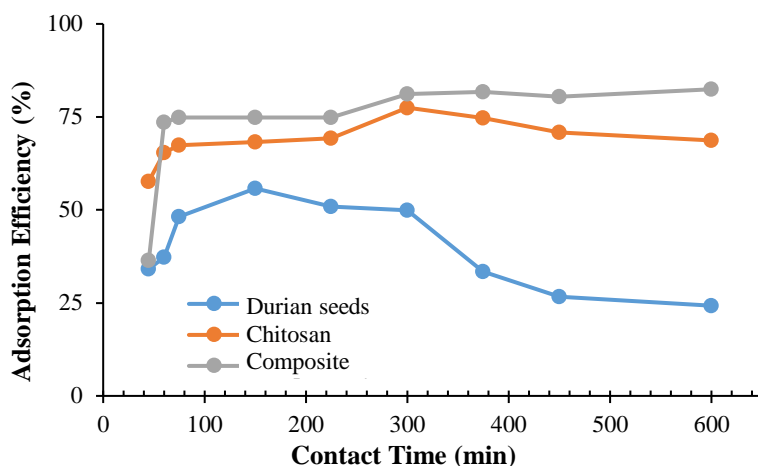

Figure 5. Adsorption efficiency of Ni(II) using chitosan, adsorbent durian seeds, and composite in various variations contact time.

The analysis of the adsorption kinetics was carried out to provide information regarding the adsorption pathway and possible mechanisms involved. Adsorption kinetics can be studied through first-order equations pseudo (pseudo-first order) and pseudo-second-order (pseudo-second order). The appropriate kinetics can be seen from the coefficient (R^2) close to 1 (Janković *et al.*, 2019). Based on the log value plot ($q_e - q_t$) to t, the value can be calculated as the adsorption rate constant (k), and the results of plotting the value of t/q_t against t can be computed as the adsorption rate constant value (k). Adsorption kinetics model parameters Ni(II) are shown in Table 1.

Table 1. Adsorption kinetics.

Kinetic Model	Parameter	Chitosan	Durian Seeds	Composite
Pseudo-second order	$K_1{}^a$ (minutes^{-1})	0.01	0.081	0.15
	q_e cal (mg/g)	-0.73	-0.69	-0.20
	q_e exp (mg/g)	4.67	3.40	2.05
	R^2	0.11	0.15	0.038
Pseudo-first order	$K_2{}^b$ (minutes^1)	0.35	0.71	1.55
	q_e cal (mg/g)	4.30	3.01	2.04
	q_e exp (mg/g)	4.67	3.40	2.05
	R^2	0.995	0.929	0.994

According to Table 1, the adsorption kinetics model suitable for showing the adsorption of Ni(II) metal ions is a pseudo-second-order kinetic model because it produces a correlation closest to 1. The q_e experimental value is closer to the q_e calculated value in the pseudo-first-order. This demonstrates that adsorption occurs via chemisorption, depending on the bonding between the chemical adsorbents and the adsorbate(Abd El Aal *et al.*, 2019). The parameter 'k' represents the kinetic constant of adsorption, indicating the speed at which the adsorption process occurs; a higher 'k' value corresponds to a faster adsorption process. According to the second-order pseudo-kinetic model, the adsorption rate constant values for Ni(II) metal ions by chitosan, durian seeds, and their composite are 0.35, 0.71, and 1.55 g/mg min, respectively. This suggests that the composite adsorbent exhibits a higher adsorption rate capability than chitosan and durian seed adsorbents. This demonstrates that adsorption occurs via chemisorption, depending on the bonding between the chemical adsorbents and the adsorbate (Abd El Aal *et al.*, 2019). The parameter 'k' represents the kinetic constant of adsorption, indicating the speed at which the adsorption process occurs; a higher 'k' value corresponds to a faster adsorption process. According to the second-order pseudo-kinetic model, the adsorption rate constant values for Ni(II) metal ions by chitosan, durian seeds,

and their composite are 0.35, 0.71, and 1.55 g/mg min, respectively. This suggests that the composite adsorbent exhibits a higher adsorption rate capability compared to chitosan and durian seed adsorbents.

Isotherm Adsorption Models

The influence of the initial concentration of the metal ion solution on adsorption capacity was examined by conducting the adsorption experiments at various concentrations, ranging from 60 to 300 mg/L. The impact of concentration on the adsorption capacity of Ni(II) metal ions on the adsorbent is depicted in Figure 6.
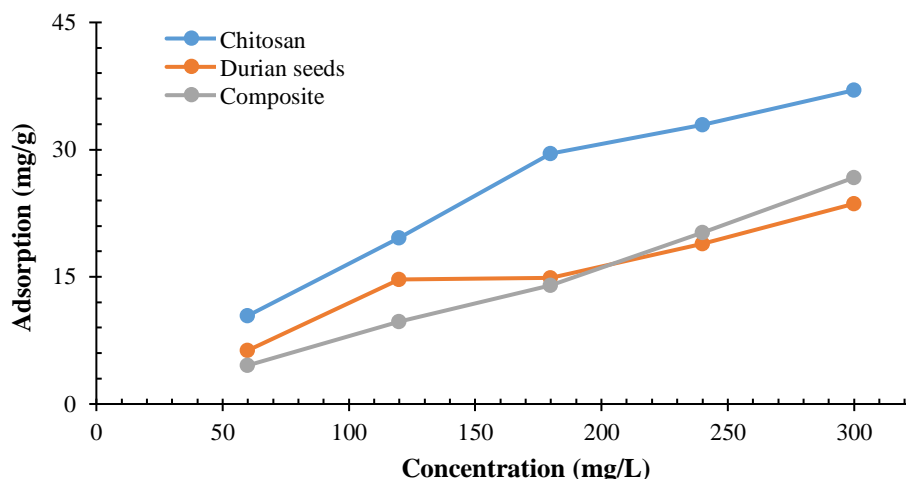

Figure 6. The adsorption capacity of Ni(II) using chitosan adsorbent, durian seed, and composite adsorbents on various concentrations of Ni(II).

Figure 6 illustrates that the adsorption capacity increases with the rising concentration of Ni(II) metal ions. The adsorption of Ni(II) metal ions on chitosan adsorbent, durian seed, and the composite increased up to a concentration of 300 mg/L, yielding adsorption capacities of 37.05 mg/g, 23.61 mg/g, and 26.69 mg/g, respectively, for each adsorbent. As the metal ion concentration increases, the adsorption capacity also increases, as more metal ions collide and bind to the active groups on the adsorbent (Rahaman *et al.*, 2021)

Adsorption isotherm control was carried out to maintain capacity maximum adsorption and identify chitosan adsorbent adsorption interactions, durian seeds, and modification of chitosan with durian seeds. Isotherm equation Langmuir adsorption is based on the assumption that single-layer adsorption on a homogeneous surface with many active sites is proportional to the area surface. Only one adsorbate molecule can be adsorbed at each site (Doondani *et al.*, 2022). Freundlich adsorption isotherm equation describes multilayer adsorption on heterogeneous surfaces and mats on the assumption that the affinity of the binding site on the adsorbent surface depends on the interactions between adsorbate ions. Therefore, the number of adsorbate ions that adsorbed increases with concentration with stronger affinity occupied first (Eze *et al.*, 2021). Langmuir adsorption isotherm is a curve of Ce to Ce/q_e, and the Freundlich isotherm is of the form curve Log Ce to Log q_e. The isotherm model is suitable when the analyzed regression coefficient has close to 1. The isotherm analysis results are shown in (Appendix 8). Mark isotherm parameters can be determined based on the lineage obtained from Langmuir and Freundlich adsorption isotherm curves. Langmuir isotherm parameters are determined based on the values of q_m, b, and RSF (Al-Ghouti *et al.*, 2019). Meanwhile, parameter values for the Freundlich isotherm are determined by the values K_F and n (Kaur *et al.*, 2021). Parameter of the adsorption isotherm model of Ni(II) metal ions is shown in Table 2.

Tabel 2. Isotherm model parameters.

Model	Parameter	Chitosan	Durian Seeds	Composite
Langmuir	q_m (mg/g)	3.267	1.410	20.145
	b (mg/L)	0.110	0.437	0.013
	Rsf	0.036	0.027	0.753
	R²	0.913	0.927	0.947
Freundlich	K_F (mg/L)	-0.765	-0.823	0.088
	n	1.093	1.881	0.618
	R²	0.991	0.907	0.797

The adsorption of Ni(II) ions by durian seed adsorbents and composites tends to conform to the Langmuir isotherm model, as it exhibits a correlation coefficient close to 1, along with an illustrative q_m value representing the maximum capacity of adsorbate adsorbed. The calculated results indicate that the adsorption capacities of chitosan adsorbent, durian seeds, and composite are 3.267, 1.410, and 20.145 mg/g, respectively. Based on the q_m value, it is evident that the chitosan/durian seed composite has a higher q_m value compared to the other adsorbents, signifying its greater adsorption capacity attributed to the bond strength between the adsorbate molecule and the adsorbent.

The RSF (separation factor) value is a critical parameter, with the following interpretations: RSF > 1 indicates a non-profitable adsorption process, RSF = 1 denotes a linear adsorption process, and 0 < RSF < 1 indicates a profitable adsorption process. A value of RSF = 0 suggests an irreversible adsorption process. The chitosan adsorbent is likely to follow the Freundlich isotherm model due to its correlation coefficient 0.991. The K_F value represents adsorption capacity and intensity for chitosan, durian seed, and the composite adsorbent, which are -0.765, -0.823, and 0.088 (mg/g), respectively. A higher K_F value corresponds to a greater adsorption ability of an adsorbent. Furthermore, the value of 'n' indicates the nature of adsorption and the strength of interaction between the adsorbate and the adsorbent. For chitosan, durian seed, and the composite, 'n' values are 1.093, 1.881, and 0.618, respectively. A smaller 'n' value suggests a stronger interaction between the adsorbate and the adsorbent.

Thermodynamic Studies

The thermodynamics of the adsorption of Ni(II) on each adsorbent was studied from the parameters of the Gibbs free energy (ΔG), entropy (ΔS), and enthalpy (ΔH), which the Van't Hoff equation can calculate the study. The thermodynamics of this adsorption was carried out at temperatures of 303 and 323 K with concentrations from 25 to 100 mg/L. Data on the adsorption results of Ni(II) at each temperature are shown in Table 3.

Table 3. Thermodynamic parameters for adsorption Ni(II).

Durian Seeds				
Concentration (mg/L)	**ΔH kJ/mol K**	**ΔS kJ/mol K**	**ΔG kJ/mol**	
			303	**323**
25	-0.628	-0.108	33.591	34.346
50	-0.505	-0.106	31.792	33.923
100	-0.338	-0.103	30.858	32.914
Chitosan				
Concentration (mg/L)	**ΔH kJ/mol K**	**ΔS kJ/mol K**	**ΔG kJ/mol**	
			303	**323**
25	-0.287	-0.184	55.616	59.036
50	-0.300	-0.254	76.861	81.954
100	-0.310	-0.781	236.580	252.216
Composite				
Concentration (mg/L)	**ΔH kJ/mol K**	**ΔS kJ/mol K**	**ΔG kJ/mol**	
			303	**323**
25	-0.264	-0.100	-30.655	-32.564
50	-0.122	-0.050	-15.484	-16.498
100	-1.235	-0.049	-16.263	-17.255

These thermodynamic parameters can be determined by plotting ln (q_e/Ce) to 1/T. Based on Table 3, the adsorbents of chitosan and durian seed adsorbent have a positive ΔG value, and this shows that the adsorption process requires greater external energy to continue (Wang *et al.*, 2020), whereas, in chitosan/durian seed composite adsorbent, the value of ΔG was negative showing that adsorption proceeds spontaneously. Comparing the values of ΔH to $T\Delta S$, the ΔH value contributed more than the $T\Delta S$ to produce a negative value on ΔG (Dotto *et al.*, 2016). Based on this, the ΔH value shows that the adsorption process releases heat (exothermic), and ΔS is marked negative. The adsorption reaction is usually chemisorption associated with ΔH values in the range of 20 – 400 kJ/mol $^{-1}$, as reported by Zhang *et al.*, 2018.

The Ni(II) metal adsorption process can be identified using the kinetic parameters, adsorption isotherm, and adsorption thermodynamics. Adsorption of Ni(II) metal is assumed to occur by chemisorption, which results in

strong covalent bonds due to coordination interactions between the adsorbent surface and the adsorbed molecule. In addition, adsorption physisorption also occurs, which involves electrostatic interactions, ion exchange, and other interactions during the process. The adsorbent may adsorb and bind Ni(II) metal because of amine functional groups from chitosan and hydroxyl groups from durian seed cellulose, according to isotherm data and adsorption kinetics. In this case, coordination interactions play a more significant role in adsorption. This process refers to covalent bonds, in which one atom shares electrons. In this interaction, cations (heavy metals) bind to groups containing lone pairs of electrons, resulting in the adsorption of cations on the surface of the adsorbate. Coordination interactions can also occur simultaneously with other interactions, including ion exchange and electrostatic interactions (Darban *et al.*, 2022).

CONCLUSION

The chitosan/durian seed composite was successfully modified in the presence of active groups –NH$_2$ and –OH, which are attractive adsorbent candidates for metal ion adsorption. The results showed that the chitosan/durian seed composite absorbed Ni(II) ions better than the chitosan adsorbent and the durian seed adsorbent, with an adsorption capacity of 26.69 mg/g and an efficiency of 89.39% at optimum conditions (pH 6, adsorbent dose 0.5 g, and contact time 60 minutes), which was higher than adsorption by the chitosan and durian seed adsorbents. The chitosan/durian seed composite and the durian seed adsorbent tended to follow the Langmuir isotherm model, whereas the chitosan adsorbent tended to follow the Freundlich isotherm model. Adsorption kinetics follows pseudo-second-order kinetics. Thermodynamic studies show that the reaction is exothermic and spontaneous.

CONFLICT OF INTEREST

There is no conflict of interest in this article.

AUTHOR CONTRIBUTION

All authors confirm responsibility for study conception and design, data collection, analysis and interpretation of results, and manuscript preparation. All authors reviewed the results and approved the final version of the manuscript.

REFERENCES

Abd El Aal, S.A., Abdelhady, A.M., Mansour, N.A., Hassan, N.M., Elbaz, F., and Elmaghraby, E.K., 2019. Physical and Chemical Characteristics of Hematite Nanoparticles Prepared Using Microwave-Assisted Synthesis and Its Application as Adsorbent for Cu, Ni, Co, Cd and Pb from Aqueous Solution. *Materials Chemistry and Physics,* 235, 121771. https://doi.org/10.1016/j.matchemphys.2019.121771.

Abdelbasir, S.M., El-Shewaikh, A.M., El-Sheikh, S.M., and Ali, O.I., 2021. Novel Modified Chitosan Nanocomposites for Co(II) Ions Removal from Industrial Wastewater. *Journal of Water Process Engineering,* 41, 102008. https://doi.org/10.1016/j.jwpe.2021.102008.

Abouhussein, D.M.N., El-Bary, A.A., Shalaby, S.H., and El Nabarawi, M.A., 2016. Chitosan Mucoadhesive Buccal Films: Effect of Different Casting Solvents on Their Physicochemical Properties. *International Journal of Pharmacy and Pharmaceutical Sciences,* 8(9), 206–213. https://doi.org/10.22159/ijpps.2016.v8i9.12999.

Adolfsson, K.H., Yadav, N., and Hakkarainen, M., 2020. Cellulose-Derived Hydrothermally Carbonized Materials and Their Emerging Applications. *Current Opinion in Green and Sustainable Chemistry,* 23, 18–24. https://doi.org/10.1016/j.cogsc.2020.03.008.

Al-Ghamdi, Y.O., 2022. Immobilization of Cellulose Extracted from Robinia Pseudoacacia Seed Fibers onto Chitosan: Chemical Characterization and Study of Methylene Blue Removal. *Arabian Journal of Chemistry,* 15(9), 104066. https://doi.org/10.1016/j.arabjc.2022.104066.

Al-Ghouti, M.A., Da'ana, D., Abu-Dieyeh, M., and Khraisheh, M., 2019. Adsorptive Removal of Mercury from Water by Adsorbents Derived from Date Pits. *Scientific Reports,* 9(1), 1–15. https://doi.org/10.1038/s41598-019-51594-y.

Alkherraz, A.M., Ali, A.K., and Elsherif, K.M., 2020. Removal of Pb (II), Zn (II), Cu (II) and Cd (II) from Aqueous Solutions by Adsorption onto Olive Branches Activated Carbon: Equilibrium and Thermodynamic Studies. *J. Chemistry International,* 6(1), 11–20. https://doi.org/10.5281/zenodo.2579465.

Anush, S.M., Chandan, H.R., Gayathri, B.H., Asma, Manju, N., Vishalakshi, B., Kalluraya, B., 2020. Graphene

Oxide Functionalized Chitosan-Magnetite Nanocomposite for Removal of Cu(II) and Cr(VI) from Waste Water. *International Journal of Biological Macromolecules,* 164, 4391–4402. https://doi.org/10.1016/j.ijbiomac.2020.09.059.

Basir, I.F., Mahatmanti, F.W., and Haryani, S., 2017. Sintesis Komposit Beads Kitosan/Arang Aktif Tempurung Kelapa Untuk Adsorpsi Ion Cu(II). *Indonesian Journal of Chemical Science,* 6(2), 181–188.

Boeykens, S.P., Redondo, N., Obeso, R.A., Caracciolo, N., and Vázquez, C., 2019. Chromium and Lead Adsorption by Avocado Seed Biomass Study Through The Use of Total Reflection X-Ray Fluorescence Analysis. *Applied Radiation and Isotopes,* 153, 108809. https://doi.org/10.1016/j.apradiso.2019.108809.

Chua, J.Y., Pen, K.M., Poi, J.V., Ooi, K.M., and Yee, K.F., 2023. Upcycling of Biomass Waste from Durian Industry for Green and Sustainable Applications: An Analysis Review in The Malaysia Context. *Energy Nexus,* 10, 100203. https://doi.org/10.1016/j.nexus.2023.100203.

Darban, Z., Shahabuddin, S., Gaur, R., Ahmad, I., and Sridewi, N., 2022. Hydrogel-Based Adsorbent Material for the Effective Removal of Heavy Metals from Wastewater: A Comprehensive Review. *Gels,* 8(5), 263. https://doi.org/10.3390/gels8050263.

Doondani, P., Gomase, V., Saravanan, D., and Jugade, R.M., 2022. Chitosan Coated Cotton-Straw-Biochar as an Admirable Adsorbent for Reactive Red Dye. *Results in Engineering,* 15, 100515. https://doi.org/10.1016/j.rineng.2022.100515.

Dotto, G. L., Rodrigues, F. K., Tanabe, E. H., Fröhlich, R., Bertuol, D. A., Martins, T. R., and Foletto, E. L., 2016. Development of Chitosan/Bentonite Hybrid Composite to Remove Hazardous Anionic and Cationic Dyes from Colored Effluents. *Journal of Environmental Chemical Engineering,* 4(3), 3230–3239. https://doi.org/10.1016/j.jece.2016.07.004.

Eze, S. I., Abugu, H. O., and Ekowo, L. C., 2021. Thermal and Chemical Pretreatment of Cassia Sieberiana Seed as Biosorbent for Pb^{2+} Removal from Aqueous Solution. *Desalination and Water Treatment,* 226, 223–241. https://doi.org/10.5004/dwt.2021.27234.

Gillmore, M. L., Gissi, F., Golding, L. A., Stauber, J. L., Reichelt-Brushett, A. J., Severati, A., Humphrey, C.A., and Jolley, D. F., 2020. Effects of Dissolved Nickel and Nickel-Contaminated Suspended Sediment on The Scleractinian Coral, Acropora Muricata. *Marine Pollution Bulletin,* 152, 110886. https://doi.org/10.1016/j.marpolbul.2020.110886.

Hammi, N., Chen, S., Dumeignil, F., Royer, S., and El Kadib, A., 2020. Chitosan as a Sustainable Precursor for Nitrogen-Containing Carbon Nanomaterials: Synthesis and Uses. *Materials Today Sustainability,* 10, 192. https://doi.org/10.1016/j.mtsust.2020.100053.

Heidari, M., Dutta, A., Acharya, B., and Mahmud, S., 2019. A Review of The Current Knowledge and Challenges of Hydrothermal Carbonization for Biomass Conversion. *Journal of the Energy Institute,* 92(6), 17791799. https://doi.org/10.1016/j.joei.2018.12.003.

Ifijen, I. H., Itua, A. B., Maliki, M., Ize-Iyamu, C. O., Omorogbe, S. O., Aigbodion, A. I., and Ikhuoria, E. U., 2020. The Removal of Nickel and Lead Ions From Aqueous Solutions Using Green Synthesized Silica Microparticles. *Heliyon,* 6(9), e04907. https://doi.org/10.1016/j.heliyon.2020.e04907.

Janković, B., Manić, N., Dodevski, V., Radović, I., Pijović, M., Katnić, Đ., and Tasić, G., 2019. Physico-Chemical Characterization of Carbonized Apricot Kernel Shell as Precursor for Activated Carbon Preparation in Clean Technology Utilization. *Journal of Cleaner Production,* 236, 117614. https://doi.org/10.1016/j.jclepro.2019.117614.

Kafle, B.P., 2020. Chapter 6 - Introduction to Nanomaterials and Application of UV–Visible Spectroscopy for Their Characterization. *Chemical Analysis and Material Characterization by Spectrophotometry,* 2020, 147–198. https://doi.org/10.1016/B978-0-12-814866-2.00006-3.

Kaur, R., Goyal, D., and Agnihotri, S., 2021. Chitosan/PVA Silver Nanocomposite for Butachlor Removal: Fabrication, Characterization, Adsorption Mechanism and Isotherms. *Carbohydrate Polymers,* 262, 117906. https://doi.org/10.1016/j.carbpol.2021.117906.

Kayalvizhi, K., Alhaji, N. M. I., Saravanakkumar, D., Mohamed, S. B., Kaviyarasu, K., Ayeshamariam, A., Al-Mohaimeed, A.M., AbdelGawwad, M.R., and Elshikh, M. S., 2022. Adsorption of Copper and Nickel by Using Sawdust Chitosan Nanocomposite Beads – A Kinetic and Thermodynamic Study. *Environmental Research,* 203, 111814. https://doi.org/10.1016/j.envres.2021.111814.

Kulkarni, R. M., Dhanyashree, J. K., Varma, E., and Sirivibha, S. P., 2022. Batch and Continuous Packed Bed Column Studies on Biosorption of Nickel (II) by Sugarcane Bagasse. *Results in Chemistry,* 4, 100328. https://doi.org/10.1016/j.rechem.2022.100328.

Kristianto, H., Daulay, N., and Arie, A. A., 2019. Adsorption of Ni(II) Ion onto Calcined Eggshells: A Study of Equilibrium Adsorption Isotherm. *Indonesian Journal of Chemistry, 19*(1), 143.

207

https://doi.org/10.22146/ijc.29200

Lestari, I., Putri, S. D. E. P., Rahayu, M. A., and Gusti, D. R., 2022. Adsorption of Mercury from Aqueous Solution on Durian (Durio zibethinus) Seed Immobilized Alginate. *EKSAKTA: Berkala Ilmiah Bidang MIPA,* 23(01), 30–41. https://doi.org/10.24036/eksakta/vol23-iss01/305.

Liakos, E. V., Mone, M., Lambropoulou, D. A., Bikiaris, D. N., and Kyzas, G. Z., 2021. Adsorption Evaluation for The Removal of Nickel, Mercury, and Barium Ions From Single-Component and Mixtures of Aqueous Solutions by Using an Optimized Biobased Chitosan Derivative. *Polymers* 13(2), 1–20. https://doi.org/10.3390/polym13020232.

Liao, J., Huang, H., 2019. Magnetic Chitin Hydrogels Prepared from Hericium Erinaceus Residues with Tunable Characteristics: A Novel Biosorbent for Cu^{2+} Removal. *Carbohydrate Polymers,* 220, 191–201. https://doi.org/10.1016/j.carbpol.2019.05.074.

Muaz, A. Z., Faiz, M., Suffian, M. Y., and Hamidi, A. A., 2014. The Study of Flocculant Characteristics for Landfill Leachate Treatment Using Starch Based Flocculant from Durio Zibethinus Seed. *Advances in Environmental Biology,* 8(15), 129–135.

El Mouhri, G., Merzouki, M., Belhassan, H., Miyah, Y., Amakdouf, H., Elmountassir, R., and Lahrichi, A., 2020. Continuous Adsorption Modeling and Fixed Bed Column Studies: Adsorption of Tannery Wastewater Pollutants Using Beach Sand. *Journal of Chemistry,* 2020, 7613484. https://doi.org/10.1155/2020/7613484.

Nunes, D., Pimentel, A., Santos, L., Barquinha, P., Pereira, L., Fortunato, E., and Martins, R., 2019. Synthesis, Design, and Morphology of Metal Oxide Nanostructures. *Metal Oxide Nanostructures*. http://dx.doi.org/10.1016/B978-0-12-811512-1.00002-3.

Pal, D. B., Singh, A., Jha, J. M., Srivastava, N., Hashem, A., Alakeel, M. A., Abd_Allah, E.F., and Gupta, V. K., 2021. Low-Cost Biochar Adsorbents Prepared from Date and Delonix Regia Seeds for Heavy Metal Sorption. *Bioresource Technology,* 339, 125606. https://doi.org/10.1016/j.biortech.2021.125606.

Pam, A.A., Elemile, O.O., Musa, D.E., Okere, M.C., Olusegun, A., Ameh, Y.A., 2023. Removal of Cu (II) Via Chitosan-Conjugated Iodate Porous Adsorbent: Kinetics, Thermodynamics, and Exploration of Real Wastewater Sample. *Results in Chemistry,* 5, 100851. https://doi.org/10.1016/j.rechem.2023.100851 .

Pavithra, S., Thandapani, G., Sugashini, S., Sudha, P. N., Alkhamis, H. H., Alrefaei, A. F., and Almutairi, M. H., 2021. Batch Adsorption Studies on Surface Tailored Chitosan/Orange Peel Hydrogel Composite for The Removal of Cr(VI) and Cu(II) Ions from Synthetic Wastewater. *Chemosphere* 271, 129415. https://doi.org/10.1016/j.chemosphere.2020.129415.

Payus, C. M., Refdin, M. A., Zahari, N. Z., Rimba, A. B., Geetha, M., Saroj, C., Gasparatos, A., Fukushi, K., and Oliver, P. A., 2019. Durian Husk Wastes as Low-Cost Adsorbent for Physical Pollutants Removal: Groundwater Supply. *Materials Today: Proceedings* 42, 80–87. https://doi.org/10.1016/j.matpr.2020.10.006.

Pohl, A., 2020. Removal of Heavy Metal Ions from Water and Wastewaters by Sulfur-Containing Precipitation Agents. *Water, Air, & Soil Pollution,* 231(10), 503. https://doi.org/10.1007/s11270-020-04863-w.

Poonam, Bharti, S. K., and Kumar, N., 2018. Kinetic Study of Lead (Pb^{2+}) Removal from Battery Manufacturing Wastewater Using Bagasse Biochar as Biosorbent. *Applied Water Science,* 8(4), 1–13. https://doi.org/10.1007/s13201-018-0765-z.

Rahaman, M. H., Islam, M. A., Islam, M. M., Rahman, M. A., and Alam, S. N., 2021. Biodegradable Composite Adsorbent of Modified Cellulose and Chitosan to Remove Heavy Metal Ions from Aqueous Solution. *Current Research in Green and Sustainable Chemistry,* 4, 100119. https://doi.org/10.1016/j.crgsc.2021.100119.

Rahayu, P., and Khabibi, K., 2016. Adsorpsi Ion Logam Nikel (II) oleh Kitosan Termodifikasi. *Jurnal Kimia Sains dan Aplikasi,* 19(1), 21–26. https://doi.org/10.14710/jksa.19.1.21-26.

Reis, E. D. S., Gorza, F. D., Pedro, G. D. C., Maciel, B. G., da Silva, R. J., Ratkovski, G. P., and de Melo, C. P., 2021. (Maghemite/Chitosan/Polypyrrole) Nanocomposites for The Efficient Removal of Cr (VI) from Aqueous Media. *Journal of Environmental Chemical Engineering,* 9(1), 104893. https://doi.org/10.1016/j.jece.2020.104893.

Shahnaz, T., Sharma, V., Subbiah, S., and Narayanasamy, S., 2020. Multivariate Optimisation of Cr (VI), Co (III) and Cu (II) Adsorption onto Nanobentonite Incorporated Nanocellulose/Chitosan Aerogel Using Response Surface Methodology. *Journal of Water Process Engineering,* 36, 101283. https://doi.org/10.1016/j.jwpe.2020.101283.

Shehap, A. M., Nasr, R. A., Mahfouz, M. A., and Ismail, A. M., 2021. Preparation and Characterizations of High Doping Chitosan/MMT Nanocomposites Films for Removing Iron From Ground Water. *Journal of Environmental Chemical Engineering,* 9(1), 104700. https://doi.org/10.1016/j.jece.2020.104700.

Sinyeue, C., Garioud, T., Lemestre, M., Meyer, M., Brégier, F., Chaleix, V., Sol, V., and Lebouvier, N., 2022. Biosorption of Nickel Ions Ni^{2+} by Natural and Modified Pinus Caribaea Morelet Sawdust. *Heliyon,* 8(2),

e08842. https://doi.org/10.1016/j.heliyon.2022.e08842.

Tandekar, S., Korde, S., and Jugade, R. M., 2021. Red Mud-Chitosan Microspheres for Removal of Coexistent Anions of Environmental Significance from Water Bodies. *Carbohydrate Polymer Technologies and Applications,* 2, 100128. https://doi.org/10.1016/j.carpta.2021.100128.

Wang, Y., Pan, J., Li, Y., Zhang, P., Li, M., Zheng, H., Zhang, X., Li, H., and Du, Q., 2020. Methylene Blue Adsorption by Activated Carbon, Nickel Alginate/Activated Carbon Aerogel, and Nickel Alginate/Graphene Oxide Aerogel: A Comparison Study. *Journal of Materials Research and Technology,* 9(6), 12443–12460. https://doi.org/10.1016/j.jmrt.2020.08.084.

Wu, Y., Pang, H., Liu, Y., Wang, X., Yu, S., Fu, D., Chen, J., and Wang, X., 2019. Environmental Remediation of Heavy Metal Ions by Novel-Nanomaterials: A Review. *Environmental Pollution,* 246, 608–620. https://doi.org/10.1016/j.envpol.2018.12.076.

Zhang, W., Zhang, S., Wang, J., Wang, M., He, Q., Song, J., Wang, H., and Zhou, J., 2018. Hybrid Functionalized Chitosan-Al_2O_3@SiO_2 Composite for Enhanced Cr(VI) Adsorption. *Chemosphere,* 203, 188–198. https://doi.org/10.1016/j.chemosphere.2018.03.188.

Zhu, F., Zheng, Y. M., Zhang, B. G., and Dai, Y. R., 2021. A Critical Review on The Electrospun Nanofibrous Membranes for The Adsorption of Heavy Metals in Water Treatment. *Journal of Hazardous Materials* 401, 123608. https://doi.org/10.1016/j.jhazmat.2020.123608.